Dalton Transactions

Accepted Manuscript

ROYAL SOCIETY OF CHEMISTRY

www.rsc.org/dalton

Synthesis of alloy AuCu Nanoparticles with the $L1_0$ Structure in an Ionic Liquid using Sputter Deposition

Shushi Suzuki[*a], Yousuke Tomita[a], Susumu Kuwabata[b,c], and Tsukasa Torimoto[*a,c]

[a] Graduate School of Engineering, Nagoya University, Furo-cho, Chikusa-ku, Nagoya 464-8603, Japan

Fax: +81-52-789-5299; Tel.: +81-52-789-2587;

[*]E-mail: shushi@apchem.nagoya-u.ac.jp, torimoto@apchem.nagoya-u.ac.jp

[b] Graduate School of Engineering, Osaka University, Suita, Osaka 565-0871, Japan

[c] Japan Science and Technology Agency, CREST, Kawaguchi, Saitama 332-0012, Japan

Abstract

Sputter deposition onto ionic liquids (ILs) was applied to synthesize AuCu bimetallic alloy nanoparticles (NPs) dispersed in 1-ethyl-3-methylimidazolium tetrafluoroborate (EMI-BF_4). A mixed target of Au and Cu materials was used for simultaneous sputter deposition onto the IL under Ar pressure of 10 Pa. Two types of heating procedures within the range of 323-573 K were examined for control of the structures of NPs, particularly addressing the phase transition of the alloy NPs from the face centered cubic (fcc) structure to the $L1_0$ structure. One was heating after the sputter deposition in N_2 at atmospheric pressure for 1 h. Another was a combination of heating during the sputter deposition and subsequent heating under Ar pressure from 0.5 to 0.8 Pa for 1 h. Although both cases exhibited lowering the phase transition temperatures compared with the temperature for the bulk, the latter procedure at 423 K only provided the NPs (approx. 5 nm) consisting of the $L1_0$ structure in the dispersed manner. A mechanism for forming the $L1_0$ structure was proposed for explaining the difference between results obtained using the two procedures.

Introduction

The study of nanocrystalline inorganic solids or nanoparticles (NPs) has been pursued to develop functional new materials in the fields of catalysis,[1-3] electronic devices,[4, 5] bio-sensors,[6, 7] fuel cells[8-10], etc. Especially, much attention has been devoted to bimetallic alloy NPs. For instance, Au–based bimetallic NPs are widely used for catalytic and electrocatalytic chemical reactions such as selective oxidation reaction of alcohols[2, 9, 11, 12] and oxygen reduction reaction(ORR).[13-15] Particularly, AuCu alloy NPs are of special interest for their catalytic functions. The AuCu NPs electrodeposited on multi-walled carbon nanotubes (AuCu-MWCNTs) showed significant current enhancement of electrocatalytic activity in the ORR, compared to that of Cu-MWCNT and Au-MWCNT.[15] The bimetallic alloy NPs showed chemical properties that depend on their sizes and structures, correlated with local distributions of elements in the NPs.[15-17] Besides, the core-shell AuCu@Pt NPs, synthesized by depositing Pt on preformed AuCu alloy NPs, exhibited superior electrocatalytic activity and excellent stability for ORR.[18] The Au component in the AuCu alloy core is crucial for stabilizing the Pt shell during ORR.

The Au–Cu system is a representative system in which several order–disorder phase transitions occur.[19] Actually, the AuCu alloy exhibits the phase transition from fcc structure (Fig. 1(a)) to $L1_0$ structure (Fig. 1(b)). In the $L1_0$ structure, the layers of Au and Cu atoms are stacked alternately in the (002) plane. Because of the difference in the atomic radii, the length along the c axis in the unit cell of the $L1_0$ structure shrinks with the c/a ratio reported as 0.931–0.938.[19] Changes in volume and hardness of AuCu alloy during the phase transition were studied for mechanical applications[20]. In the case of magnetic alloys of FeNi[21], FePt[22, 23] and CoPt[24], magnetic anisotropy was attractive for applications in the field of magnetic recording and magneto-electronics. Influence of order-disorder phase transition was also reported on catalytic property[17] and surface plasmon resonance[25], although relations between the $L1_0$ structure and these properties should be more clarified. Since mixing other phases and multivalent structures in the NPs prevent to exhibit intrinsic character of the $L1_0$ structure, it is important to improve methodology to control the structural formation.

Formation of the $L1_0$ structure in the bulk material requires heat treatment at certain temperatures

higher than 573 K, with the phase transition from the fcc structure formed at lower temperatures. In the case of NPs, however, high-temperature heat treatment is disadvantageous to prepare NPs with their sizes kept at a few nanometers in a dispersed manner. Indeed, formation of the $L1_0$ structure in the AuCu NPs stabilized by poly[vinyl-2-pyrrolidone (PVP) was confirmed between 473 K and 673 K in solution, but the average diameter of these NPs exceeded 15 nm.[26, 27] Thus, great attention has been devoted to synthesis of $L1_0$-type NPs in a dispersive manner. Nevertheless, it was reported recently that the rate of phase transition from the fcc to the $L1_0$ structures in the PVP-stabilized AuCu NPs can be accelerated under a hydrogen atmosphere at 433 K.[28] Results show that the key to producing ordered nanoalloys is the treatment of hydrogen to induce a phase transition at low temperatures with suppression of the aggregation of NPs,[28-30] as well as the preparation of atomically well-mixed alloys as precursors. Moreover, thermodynamic calculations based on the modified analytical embedded atom method (MAEAM) showed that the formation of Au–Cu divacancies in the $L1_0$ structure was more favorable than the other type of divacancy formation between Au–Au and Cu–Cu.[31] We inferred the possibility that the AuCu alloy preferred to maintain its composition at certain equivalent states. Furthermore, the first principle calculations showed that the Au–Cu interaction has negative mixing enthalpies[32]. The $L1_0$ structure in the AuCu alloy NPs was identified as the most stable phase in terms of energy.[32, 33]

According to these experimental and theoretical results, we expected that the $L1_0$ structure of AuCu can be prepared at low temperatures of less than 500 K if a mixture of Au and Cu atoms can be introduced into reactive media before the formation of Au–Au and Cu–Cu bonds. In this regard, sputter deposition onto ionic liquids (ILs) is a suitable technique to produce the mixture in the reactive media. Previously, our group[34, 35] and others[36-39] reported that the sputter deposition technique is useful to synthesize NPs in ILs at room temperature. Actually, synthesis of highly dispersed Au, Ag, and their alloy NPs dispersed in ILs was conducted by the sputter deposition at room temperature.[34, 35, 40-43] Similarly to the Au–Cu interaction, the Au–Ag interaction has negative mixing enthalpies, which might be a cause of alloy formation at room temperature. The combinatorial approach for synthesis of AuCu alloy NPs was reported recently using co-sputtering of two separate targets onto 1-butyl-3-methylimidazolium

trifluoromethanesulfonylamide (BMI-TFSA)[39]. The Au–Cu ratio of NPs depended strongly on distances between targets and a sampling cavity array filled with the IL. Thus, spontaneous formation of the $L1_0$ structure in the AuCu alloy NPs can be anticipated if Au and Cu atoms could be injected into the ILs.

Here, the report describes the synthesis of AuCu alloy NPs by sputter deposition in 1-ethyl-3-methylimidazolium tetrafluoroborate (EMI-BF_4) and the phase transition of the AuCu alloy NPs from the fcc structure to the $L1_0$ structure by adopting two types of heat treatments, showing that the $L1_0$ structure in the AuCu alloy NPs of 5 nm in diameter could be synthesized without aggregation.

Experimental

As the IL, 1-ethyl-3-methylimidazolium tetrafluoroborate (EMI-BF_4) (Kanto Chemical Co., Inc.) was used. The IL was dried for 3 h at 393 K under vacuum conditions before use. The dried IL was spread on a glass plate set in a sputter coater (SC-701HMCII; Sanyu Electron Co., Ltd.). A sputtering target was placed 38 mm distant from the glass plate. The typical applied voltage between them was about 0.5 kV. For simultaneous sputtering of Au and Cu, a mixed target material was prepared by sticking several radial-shaped flakes of Cu foil (99.99% in purity) on a round Au foil (99.99% in purity) with electrically conductive adhesive tape. As presented in Fig. 2, sputtering target materials of three types with different ratios of Au:Cu were used, in addition to two pure targets of Au and Cu. Here, the fraction of total Au area on the mixed target is defined as $f_{Au} = A_{Au}/(A_{Au} + A_{Cu})$, where A_{Au} and A_{Cu} respectively stand for the total areas of Au and Cu at the top-most plane on the target. Sputtering deposition of Au and Cu onto EMI-BF_4 was conducted for 300 s with a current of 40 mA under argon pressure of 10 Pa.

In addition to using a mixed target of Au and Cu materials for simultaneous sputter deposition onto the IL, two types of heating procedures were applied for controlling the NP structures with the phase transition of the alloy NPs from the fcc structure to the $L1_0$ structure. The first procedure, designated as X, is a combination of sputter deposition onto the IL at room temperature under Ar pressure of 10 Pa and heating at certain temperatures from 323 K to 573 K in N_2 at atmospheric pressure for 1 h. Since the heating was conducted in a separate apparatus, samples were exposed to the air once before the heating.

The second procedure, designated as Y, is a combination of sputter deposition onto the IL and heating at certain temperatures from 323 K to 473 K under Ar pressure from 0.5 to 0.8 Pa for 1 h. Procedure Y was conducted in a unit of the sputter coater without exposure to air.

The NPs formed in the IL were observed using TEM (H-7650, Hitachi Ltd.) operated at acceleration voltage of 100 kV. Samples for TEM observation were prepared by dipping a copper grid with amorphous carbon overlayers (#10-1012, Okenshoji Co. Ltd.) into the IL including NPs. The excess amount of IL was rinsed by acetonitrile with subsequent drying *in vacuo*. Particle sizes were determined using image analysis software such as ImageJ developed at the National Institutes of Health (NIH). The chemical composition of the NPs was determined using X-ray fluorescence (XRF; EDXL300, Rigaku Co.). As samples for XRF analysis, the IL including NPs was measured in a He atmosphere. The crystalline structure of NPs was investigated using X-ray diffraction (XRD; RINT2100HL, Rigaku Co.) equipped with a Cu Kα X-ray tube. Samples for XRD measurements were prepared by isolation of NPs from the IL. After adding a large amount of methanol to the IL, precipitates were collected by centrifugation and were dried *in vacuo*. UV–Vis spectra of the NPs were measured using a UV–Vis spectrometer (Agilent8453, Agilent Technologies Inc.). A quartz cell with a light path length of 0.1 mm was used. The ILs without the sputtering treatment were used as blanks for the measurements.

Results and Discussion

1) Preparation of AuCu alloy NPs by sputter deposition in the IL

Figures 3(a)–3(e), respectively show TEM images of the NPs obtained by sputtering of the targets with the f_{Au} of 0, 0.25, 0.50, 0.75, and 1. The particle size distribution in each case is also shown at the right side of corresponded image data. Although the NPs obtained from the mixed targets (f_{Au}=0.25, 0.50, and 0.75) showed slightly wider standard deviations than those in cases of pure Cu (f_{Au}=0) and pure Au (f_{Au}=1), the average diameters of the NPs in all cases were 2–4 nm. The NPs were dispersed in the IL of EMI-BF_4 without aggregation, as observed in our previous studies.[34, 35, 40-43]

The compositional ratios of Au:Cu of the NPs analyzed using XRF show mostly equivalent

values to the fraction of the mixed target in each case, as described in Table I. For instance, the mixed target with f_{Au}=0.50 provided the composition ratio of Au:Cu as 46:54 for the NPs dispersed in the IL. Furthermore, the UV–Vis spectra on the NPs revealed a clue related to the formation of the alloy NPs. Figures 4(a) (i)–(v) show UV–Vis spectra for the NPs obtained from the targets with f_{Au}=0, 0.25, 0.50, 0.75, and 1, respectively. Although clear surface plasmon resonance (SPR) peaks at the wavelength of about 560 nm and 520 nm were observed in the cases of pure Cu (f_{Au}=0) and pure Au (f_{Au}=1)[25, 46, 47], ambiguous peak-like features marked by arrows were observed in the spectra for the NPs obtained from the mixed targets with f_{Au}=0.25, 0.50, and 0.75. The wavelengths denoted by the arrows were blue-shifted between two SPR peaks for Au and Cu with increasing f_{Au} value, as presented in Fig. 4(b). In the previous study, the Au–Ag NPs[44, 45] and the Au–Cu NPs[35] with varying Au contents showed linear dependency of the SPR peak position. Thus, we judged that the mixed targets (f_{Au}=0.25, 0.50, and 0.75) provided Cu_3Au, AuCu, and Au_3Cu alloy NPs in a similar fashion, respectively, because the shifting in Fig. 4(b) also showed linear dependency.

2) Heating the AuCu alloy NPs in accordance with the X procedure

The AuCu NPs with f_{Au} of 0.50 were used to prepare NPs with the $L1_0$ structure by heat treatment. Figure 5 presents XRD profiles of the AuCu alloy NPs prepared in accordance with the X procedure. The XRD profile of the as-synthesized NPs is also shown in Fig. 5. The bar graphs attached at the bottom of the figure are references describing the peaks of the fcc structure and the $L1_0$ structure. A prominent peak in the XRD profile for the as-synthesized NPs was assigned to the (111) peak of the fcc structure. The crystallite diameter (d) estimated from the full width at half-maximum (B) of the (111) Bragg peak (θ) using Scherrer equation ($d = 0.9\lambda/B\cos\theta$)[3, 46] was about 2 nm. The parameter of λ is the wavelength of X-ray light. The crystallite diameter was smaller than the particle size estimated from the TEM image in Fig. 3(c), indicating that it was deduced that the as-synthesized NPs had a disordered fcc structure involving grain boundaries. Although the $L1_0$ structure was not formed spontaneously at room temperature during the sputter deposition process, the (111) peak of the fcc structure became sharper with increasing temperature of the

heat treatment. Finally, the peak was shifted to the peak position of the $L1_0$ structure. As Table II shows, the composition of the NPs analyzed by XRF was kept almost constant during the heating process. These results show that the disordered-fcc structure of the alloy NPs were transformed to the ordered-$L1_0$ structure at temperatures higher than 473 K. However, after transforming the $L1_0$ structure, the NPs invariably aggregated and increased in size with exceeding 20 nm in diameter under these temperature conditions. A series in Figs. 6(a)–6(f) shows TEM images of AuCu NPs after heating at 323, 373, 423, 473, 523, and 573 K. The particle sizes in Figs. 6(d)–6(f) were larger than the sizes in Figs. 6(a)–6(c). The AuCu NPs increased their size drastically at temperatures higher than 473 K, although the phase transition to the $L1_0$ structure occurred at the temperature. The cause of particle growth was probably particle aggregation or sintering of the nanoparticles observed in Figs. 6(a)–6(c). A possible mechanism was suggested in the latter section. The crystallite diameters estimated from the XRD profile in Fig. 5 were greater than 5 nm for the $L1_0$ structure, indicating that the grown NPs involved grain boundaries. Therefore, it was difficult to obtain the AuCu NPs with the $L1_0$ structure in a dispersed manner by the heating procedure of X.

3) Heating the AuCu alloy NPs in accordance with the Y procedure

To improve the heat treatments, the Y procedure was adopted to prepare the $L1_0$ structure in the NPs without aggregation. Here, the effect of heat treatments was examined step by step using the mixed targets of f_{Au} = 0.50. Figure 7(a) presents XRD profiles of the NPs obtained by heating during the sputter deposition under Ar pressure of 10 Pa, whereas Fig. 7(b) shows XRD profiles of the NPs obtained by additional heating for 1 h under Ar pressure of 0.5–0.8 Pa with keeping the same temperatures for the sputter deposition. Cases without heat treatment are also presented in these figures. The bar graphs in figures at the bottom and the top are references respectively show peak positions of the fcc structure and the $L1_0$ structure. Dashed lines in each figure show the (111) peak position in the fcc structure. Data in Fig. 7(b) were processed using a smoothing function to clarify the peak shifting, although the signal-to-noise ratio was similar to that shown in Fig. 7(a).

Figure 7(a) presents results of heating obtained at 323, 373, and 423 K and without heating,

indicating that similar peak profiles correspond to the fcc structure. No effect of heating was observed on the phase transition of the NPs during sputter deposition. Fig. 7(b) represents the effects of the following heating clearly as a peak shift in the XRD profile at 423 K, indicating that the $L1_0$ structure formed in the NPs. Because the crystallite diameter estimated from the XRD profile at 423 K was 4 nm, the heat treatments in the Y procedure were more effective in lowering temperatures for the phase transition of the AuCu alloy NPs.

The dispersed state and the size distributions of the obtained NPs were investigated using TEM observations. Figure 8 shows TEM images of the NPs corresponded to Fig. 7(a), whereas Fig. 9 shows TEM images of the NPs corresponded to Fig. 7(b). The average sizes of the NPs observed in Fig. 8 are 2.5–3.0 nm. Because the appearances of the NPs show no distinctive difference among them in terms of shape or size, heating at less than or equal to 423 K during the sputter deposition did not influence the dispersed state of the NPs. Besides, the further 1h heating at the same temperatures did not affect the dispersed states of the NPs, as shown in Fig. 9. It means that the AuCu alloy NPs with the $L1_0$ structure could be synthesized by heating at 423 K in the dispersive manner, though the NPs grew from 3 nm to 5 nm in diameter. The heating at 473 K, however, provided particle aggregation, as presented in Fig. 10. The NP size exceeded 20 nm, which was as large as the NPs in the case of 473 K of the X procedure, as shown in Fig. 6(d).

The compositional ratios of Au:Cu of the NPs obtained by the Y procedure were confirmed, as presented in Table III except in the case of 473 K. Although the compositions of the NPs were in slightly Cu-rich states, the content of Au in the NPs during the heating was kept constant at about 40–46%. The Cu-rich states appeared to be caused by an unexpected error in the fraction rate of the Au area on a mixed target. Thus, the heat treatment at 423 K through the Y procedure also did not affect the compositions in the alloy NPs with the $L1_0$ structure.

4) Possible mechanism for formation of the $L1_0$ structure in the AuCu alloy NPs at 423 K

Through these experiments, results showed that the phase transition temperatures of the NPs

decreased in both cases, compared with the temperature higher than 573 K for the phase transition in the bulk. We propose a possible mechanism by which the alloy AuCu NPs with the $L1_0$ structure was obtained even at 423 K, as presented in Fig. 11. For the X procedure as presented in Fig. 11(a), the heat treatment was applied to the NPs, of which the size was increased already to about 3 nm, resulting in formation of the $L1_0$ structure at 473 K with particle aggregation. For the Y procedure as presented in Fig. 11(b), heating at 423 K was applied from the start of the sputter deposition with subsequent heat treatment at 423 K for 1 h.

The coupling of Au and Cu is energetically favored, compared to forming the Cu–Cu bond and the Au–Au bond, as calculated theoretically in previous studies[32, 33]. Thus, it was proposed that a seed of the $L1_0$ structure could be formed during sputter deposition onto the IL at 423 K. Then, the seed of the $L1_0$ structure promoted the growth of the $L1_0$ structure in the NPs during subsequent annealing in the IL. In contrast, the phase transition required higher temperature than 423 K in the X procedure, because no nucleus may be formed for the growth of the $L1_0$ structure. Our results suggest that controlling the Au–Cu bond was important even at the initial stage of particle growth process. The concept was commonly proposed in the previous paper, which shows the value of hydrogen treatment to control the rate of phase transition from the fcc to the $L1_0$ structures in the PVP-stabilized AuCu NPs.[30] The reductive ambient under low vacuum condition in our case might have a similar effect of hydrogen treatment on the phase transition rate.

Because the difference in the particle aggregation between the X and Y procedures was not observed clearly, thermally induced diffusion of the NPs might be a cause of the particle aggregation. In addition, oxidation of the NPs presents a possible cause, because surfaces of the NPs was not covered with organic molecules as so-called stabilized agents. Indeed, the NPs were exposed to the air at certain intervals between the sputtering deposition and the heating processes in the X procedure, and the low pressure of oxygen might remain under vacuum condition in the Y procedure. Therefore, it was elucidated that the oxidized thin layer surrounding the NPs has affinity to form the aggregates, providing uncontrollable jumping between the size distributions of the NPs in the 50 K range of 423–473 K.

Conclusions

Sputter deposition was applied to synthesize AuCu bimetallic NPs dispersed in EMI-BF_4. To control the structures in the NPs, two types of heating procedures, designated as X and Y, were examined, particularly addressing the phase transition of the alloy NPs from the fcc structure to the $L1_0$ structure. Through the sputter deposition and heat treatments in both cases, results showed that the phase transition temperatures of the NPs decreased compared with temperatures higher than 573 K for the bulk. Particularly, the Y procedure at 423 K can provide NPs (ca. 5 nm) consisting of the $L1_0$ structure in a dispersed manner, although further experiments are necessary to explain the mechanism. We propose that sputter deposition onto ILs has further potential for application to the synthesis of various structurally ordered alloy NPs such as FePt and CoPt NPs in a dispersed manner for application to terabit data storage.

Acknowledgments

This work was partially supported by a Grant-in-Aid for Scientific Research for Young Scientist Promotion (A) (No. 20686004) and by a Funding Program for Next Generation World-Leading Research (NEXT Program) (No. GR054) from Japan Society for the Promotion of Science (JSPS).

References

1. F. X. Liang, H. Q. Zhu, Z. F. Qin, G. F. Wang and J. G. Wang, *Prog. Chem.*, 2008, **20**, 1453-1464.
2. C. L. Bracey, P. R. Ellis and G. J. Hutchings, *Chem. Soc. Rev.*, 2009, **38**, 2231-2243.
3. A. Z. Moshfegh, *J. Phys. D: Appl. Phys.*, 2009, **42**.
4. E. Cattaruzza, G. Battaglin, F. Gonella, R. Polloni, B. F. Scremin, G. Mattei, P. Mazzoldi and C. Sada, *Appl. Surf. Sci.*, 2007, **254**, 1017-1021.
5. K. Maeda, N. Okabayashi, S. Kano, S. Takeshita, D. Tanaka, M. Sakamoto, T. Teranishi and Y. Majima, *Acs Nano*, 2012, **6**, 2798-2803.
6. J. D. Zhang, Q. J. Chi, T. Albrecht, A. M. Kuznetsov, M. Grubb, A. G. Hansen, H. Wackerbarth, A. C. Welinder and J. Ulstrup, *Electrochim. Acta*, 2005, **50**, 3143-3159.
7. A. Gutes, C. Carraro and R. Maboudian, *Electrochim. Acta*, 2011, **56**, 5855-5859.
8. H. S. Liu, C. J. Song, L. Zhang, J. J. Zhang, H. J. Wang and D. P. Wilkinson, *J. Power Sources*, 2006, **155**, 95-110.
9. M. Sankar, N. Dimitratos, P. J. Miedziak, P. P. Wells, C. J. Kiely and G. J. Hutchings, *Chem. Soc. Rev.*, 2012, **41**, 8099-8139.

10. S. Zhang, Y. Y. Shao, G. P. Yin and Y. H. Lin, *J. Mater. Chem. A*, 2013, **1**, 4631-4641.
11. C. L. Bracey, A. F. Carley, J. K. Edwards, P. R. Ellis and G. J. Hutchings, *Catal. Sci. Technol.*, 2011, **1**, 76-85.
12. J. C. Bauer, G. M. Veith, L. F. Allard, Y. Oyola, S. H. Overbury and S. Dai, *ACS Catalysis*, 2012, **2**, 2537-2546.
13. Y. H. Bing, H. S. Liu, L. Zhang, D. Ghosh and J. J. Zhang, *Chem. Soc. Rev.*, 2010, **39**, 2184-2202.
14. V. Mazumder, Y. Lee and S. H. Sun, *Adv. Funct. Mater.*, 2010, **20**, 1224-1231.
15. C. C. Bakir, N. Sahin, R. Polat and Z. Dursun, *J. Electroanal. Chem.*, 2011, **662**, 275-280.
16. J. C. Bauer, D. Mullins, M. J. Li, Z. L. Wu, E. A. Payzant, S. H. Overbury and S. Dai, *Phys. Chem. Chem. Phys.*, 2011, **13**, 2571-2581.
17. J. Yin, S. Y. Shan, L. F. Yang, D. Mott, O. Malis, V. Petkov, F. Cai, M. S. Ng, J. Luo, B. H. Chen, M. Engelhard and C. J. Zhong, *Chem. Mater.*, 2012, **24**, 4662-4674.
18. J. H. Yang, X. J. Chen, X. F. Yang and J. Y. Ying, *Energ. Environ. Sci.*, 2012, **5**, 8976-8981.
19. H. Okamoto, D. J. Chakrabarti, D. E. Laughlin and T. B. Massaiski, *Bull. Alloy. Phase. Diagr.*, 1987, **8**, 454-473.
20. T. Anraku, I. Sakaihara, T. Hoshikawa and M. Taniwaki, *Mater. Trans.*, 2009, **50**, 683-688.
21. T. Kojima, M. Ogiwara, M. Mizuguchi, M. Kotsugi, T. Koganezawa, T. Ohtsuki, T. Y. Tashiro and K. Takanashi, *J. Phys.: Condens. Matter*, 2014, **26**.
22. T. Shimatsu, Y. Inaba, H. Kataoka, J. Sayama, H. Aoi, S. Okamoto and O. Kitakami, *J. Appl. Phys.*, 2011, **109**.
23. W. Y. Ding, S. Ishiguro, R. Ogatsu and D. Y. Ju, *Appl. Surf. Sci.*, 2012, **258**, 7976-7981.
24. H. Akamine, S. Farjami, M. Mitsuhara, M. Nishida, T. Fukuda and T. Kakeshita, *Mater. Trans.*, 2013, **54**, 1715-1718.
25. S. Pramanik, M. K. Mishra and G. De, *CrystEngComm*, 2014, **16**, 56-63.
26. A. K. Sra and R. E. Schaak, *J. Am. Chem. Soc.*, 2004, **126**, 6667-6672.
27. R. E. Schaak, A. K. Sra, B. M. Leonard, R. E. Cable, J. C. Bauer, Y. F. Han, J. Means, W. Teizer, Y. Vasquez and E. S. Funck, *J. Am. Chem. Soc.*, 2005, **127**, 3506-3515.
28. M. Yamauchi, K. Okubo, T. Tsukuda, K. Kato, M. Takata and S. Takeda, *Nanoscale*, 2014, **6**, 4067-4071.
29. M. Okada, A. Kamegawa, J. Nakahigashi, A. Yamaguchi, A. Fujita and M. Yamauchi, *Mater. Sci. Eng. B-Adv.*, 2010, **173**, 253-259.
30. M. Yamauchi and T. Tsukuda, *Dalton Trans.*, 2011, **40**, 4842-4845.
31. Z. L. Lin, Y. Zhang, J. M. Zhang and K. W. Xu, *Phys. Status Solidi. B*, 2011, **248**, 897-903.
32. V. Ozolins, C. Wolverton and A. Zunger, *Phys. Rev. B*, 1998, **57**, 6427-6443.
33. L. G. Ferreira, V. Ozolins and A. Zunger, *Phys. Rev. B*, 1999, **60**, 1687-1696.
34. T. Torimoto, K. Okazaki, T. Kiyama, K. Hirahara, N. Tanaka and S. Kuwabata, *Appl. Phys. Lett.*, 2006, **89**, 243117.
35. S. Kuwabata, T. Tsuda and T. Torimoto, *J. Phys. Chem. Lett.*, 2010, **1**, 3177-3188.
36. H. Wender, L. F. de Oliveira, P. Migowski, A. F. Feil, E. Lissner, M. H. G. Prechtl, S. R. Teixeira and J.

Dupont, *J. Phys. Chem. C*, 2010, **114**, 11764-11768.

37. Y. Hatakeyama, S. Takahashi and K. Nishikawa, *J. Phys. Chem. C*, 2010, **114**, 11098-11102.
38. Y. Hatakeyama, K. Onishi and K. Nishikawa, *RSC Advances*, 2011, **1**, 1815-1821.
39. D. König, K. Richter, A. Siegel, A.-V. Mudring and A. Ludwig, *Adv. Funct. Mater.*, 2014, **24**, 2049-2056.
40. K. Okazaki, T. Kiyama, K. Hirahara, N. Tanaka, S. Kuwabata and T. Torimoto, *Chem. Commun.*, 2008, 691-693.
41. T. Tsuda, T. Kurihara, Y. Hoshino, T. Kiyama, K. Okazaki, T. Torimoto and S. Kuwabata, *Electrochemistry*, 2009, **77**, 693-695.
42. K. Okazaki, T. Kiyama, T. Suzuki, S. Kuwabata and T. Torimoto, *Chem. Lett.*, 2009, **38**, 330-331.
43. S. Suzuki, T. Suzuki, Y. Tomita, M. Hirano, K. Okazaki, S. Kuwabata and T. Torimoto, *Crystengcomm*, 2012, **14**, 4922-4926.
44. T. Endo, T. Yoshimura and K. Esumi, *J. Colloid Interf. Sci.*, 2005, **286**, 602-609.
45. A. K. Sharma and G. J. Mohr, *J. Phys. D: Appl. Phys.*, 2008, **41**, 055106.
46. U. Holzwarth and N. Gibson, *Nat. Nanotechnol.*, 2011, **6**, 534-534.

Figure Captions

Figure 1 a) The fcc structure and b) the $L1_0$ structure models in AuCu alloy materials.

Figure 2 Schematic illustrations of AuCu binary targets with different compositions of f_{Au}. The value of f_{Au} is defined as $f_{Au} = A_{Au}/(A_{Au} + A_{Cu})$, where A_{Au} and A_{Cu} respectively stand for the total areas of Au and Cu parts exposed on the targets.

Figure 3 TEM images and size distributions of NPs obtained by sputter deposition in EMI-BF_4 with the target fractions of (a) $f_{Au} = 0$, (b) $f_{Au} = 0.25$, (c) $f_{Au} = 0.50$, (d) $f_{Au} = 0.75$, and (e) $f_{Au} = 1.0$.

Figure 4 (a) UV-Vis absorption spectra of EMI-BF_4 including the NPs obtained by sputter deposition with the target fractions of (i) $f_{Au} = 0$, (ii) $f_{Au} = 0.25$, (iii) $f_{Au} = 0.50$, (iv) $f_{Au} = 0.75$, and (v) $f_{Au} = 1.0$. Arrows indicate possible peak top positions of surface plasmon resonance (SPR) observed in the spectra of (ii), (iii), and (iv). (b) Wavelengths of the peak tops in the spectra from (i)–(v) are shown as a function of Au content in the obtained NPs.

Figure 5 XRD profiles of the AuCu alloy NPs heated at (a) 323 K, (b) 373 K, (c) 423 K, (d) 473 K, (e) 523 K, and (f) 573 K in accordance with the X procedure (see the text) are shown, as well as the XRD profile of the as-synthesized NPs. The bar graphs attached at the bottom are references describing the peak positions of the fcc structure and the $L1_0$ structure. The NPs were synthesized using the mixed targets of $f_{Au} = 0.50$.

Figure 6 TEM images of NPs heated at (a) 323 K, (b) 373 K, (c) 423 K, (d) 473 K, (e) 523 K, and (f) 573 K in accordance with the X procedure. The NPs were synthesized using the mixed targets of $f_{Au} = 0.50$.

Figure 7 XRD profiles of the NPs obtained (a) by application of heating during the sputter deposition and (b) by application of the continuous heating for 1 h after the sputter deposition through the Y procedure.

Cases without heat treatment are also shown in these figures. The bar graphs in each figure at the bottom and the top are references describing the peak positions of the fcc structure and the $L1_0$ structure, respectively. A dashed line in each figure shows the (111) peak position in the fcc structure. The NPs were synthesized using the mixed targets of $f_{Au} = 0.50$.

Figure 8 TEM images and size distributions of NPs obtained through the first heating step in the Y procedure at (a) 323 K, (b) 373 K, and (c) 423 K. The heating as the first step was conducted during the sputter deposition onto the IL. The NPs were synthesized using the mixed targets of $f_{Au} = 0.50$.

Figure 9 TEM images and size distributions of NPs obtained through the whole process in the Y procedure at (a) 323 K, (b) 373 K, and (c) 423 K. The second step of subsequent heating was conducted for 1 h. The NPs were synthesized using the mixed targets of $f_{Au} = 0.50$.

Figure 10 TEM image of NPs obtained through the whole process in the Y procedure at 473 K. The NPs were synthesized using the mixed targets of $f_{Au} = 0.50$.

Figure 11 Mechanism on the formation of the $L1_0$ structure in the AuCu alloy NPs in EMI-BF_4 by application of (a) the X procedure at 473 K and (b) the Y procedure at 423 K.

Table I XRF data on compositional ratio of Au:Cu in the obtained NPs from the mixed targets of f_{Au} = 0.25, f_{Au} = 0.50, and f_{Au} = 0.75.

f_{Au}	0.25	0.50	0.75
Au ratio / %	30	46	81
Cu ratio / %	70	54	19

Table II XRF data on compositional ratio of Au:Cu in the NPs heated in accordance with the X procedure. Data on the as-synthesized NPs were also shown in the far left column labeled as "room temperature (RT)".. The NPs were synthesized using the mixed targets of $f_{Au} = 0.50$.

Temperature / K	RT	323	373	423	473	523	573
Au ratio / %	46	57	56	51	52	48	48
Cu ratio / %	54	43	44	50	48	52	52

Table III XRF data on compositional ratio of Au:Cu in the NPs heated in accordance with the Y procedure. The data on the NPs without heating was also shown in the far left column labeled as "w/o-h". The NPs were synthesized using the mixed targets of f_{Au} = 0.50.

Temperature / K	w/o-h	323	373	423
Au ratio / %	46	42	41	40
Cu ratio / %	54	58	59	60

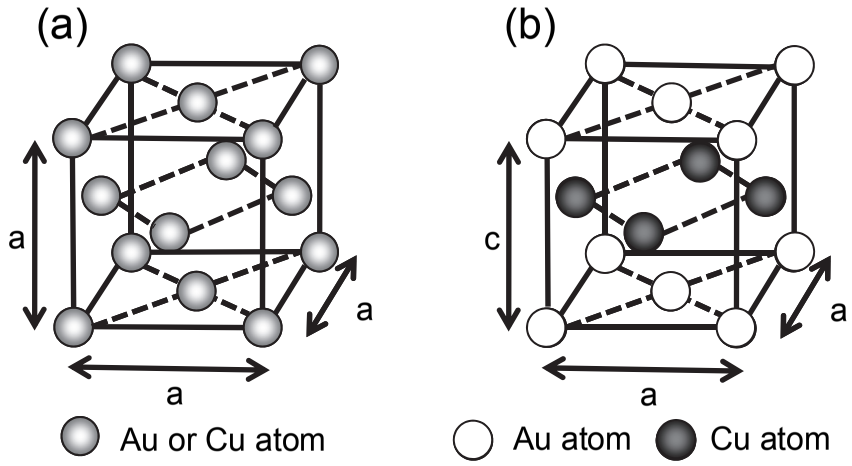

Fig. 1 a) The fcc structure and b) the $L1_0$ structure models in AuCu alloy materials.

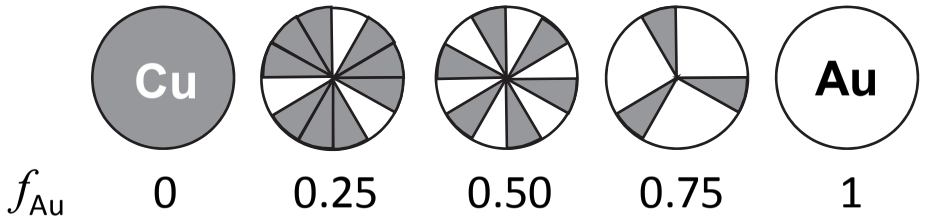

Fig. 2 Schematic illustrations of AuCu binary targets with different compositions of f_{Au}. The value of f_{Au} is defined as $f_{Au} = A_{Au}/(A_{Au} + A_{Cu})$, where A_{Au} and A_{Cu} respectively stand for the total areas of Au and Cu parts exposed on the targets.

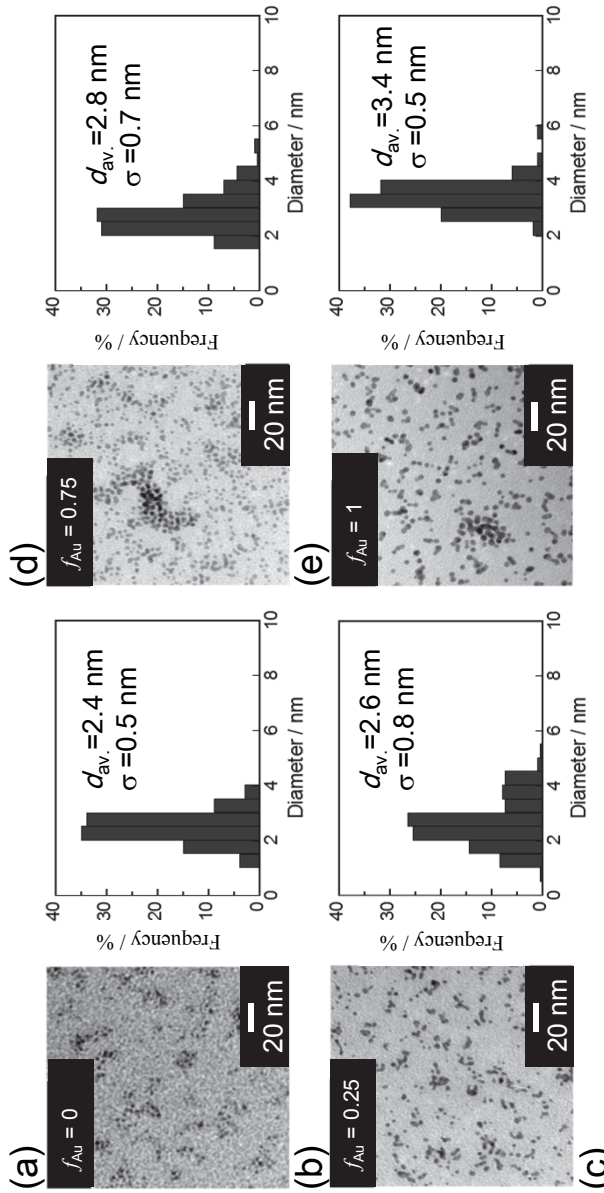

Fig. 3 TEM images and size distributions of NPs obtained by sputter deposition in EMI-BF_4 with the target fractions of (a) f_{Au} = 0, (b) f_{Au} = 0.25, (c) f_{Au} = 0.50, (d) f_{Au} = 0.75, and (e) f_{Au} = 1.

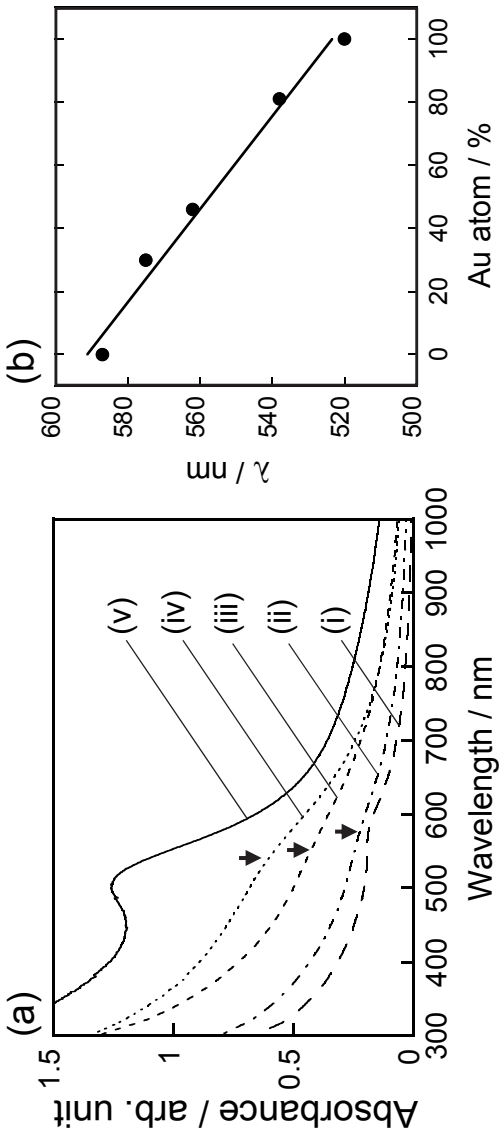

Fig. 4 (a) UV-Vis absorption spectra of EMI-BF_4 including the NPs obtained by sputter deposition with the target fractions of (i) $f_{Au} = 0$, (ii) $f_{Au} = 0.25$, (iii) $f_{Au} = 0.50$, (iv) $f_{Au} = 0.75$, and (v) $f_{Au} = 1$. Arrows indicate possible peak top positions of surface plasmon resonance (SPR) observed in the spectra of (ii), (iii), and (iv). (b) Wavelengths of the peak tops in the spectra from (i)–(v) are shown as a function of Au content in the obtained NPs.

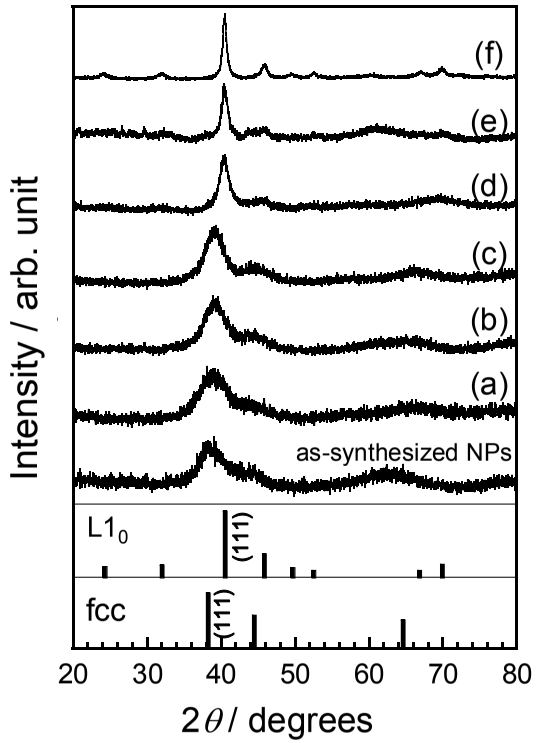

Fig. 5 XRD profiles of the AuCu alloy NPs heated at (a) 323 K, (b) 373 K, (c) 423 K, (d) 473 K, (e) 523 K, and (f) 573 K in accordance with the X procedure (see the text) are shown, as well as the XRD profile of the as-synthesized NPs. The bar graphs attached at the bottom are references describing the peak positions of the fcc structure and the $L1_0$ structure. The NPs were synthesized using the mixed targets of $f_{Au} = 0.50$.

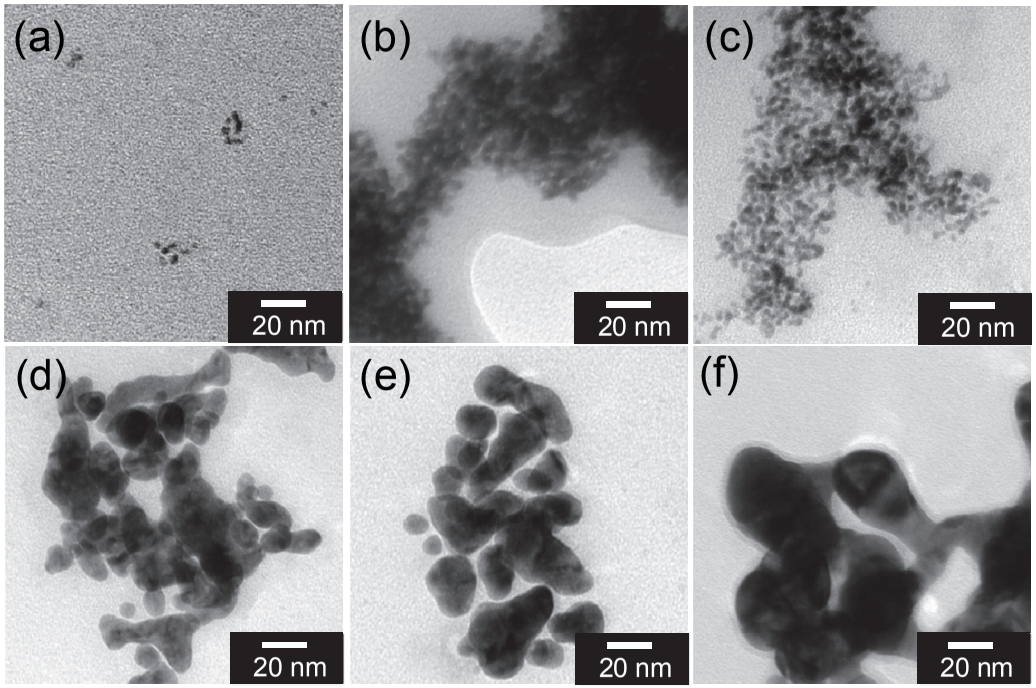

Fig. 6 TEM images of NPs heated at (a) 323 K, (b) 373 K, (c) 423 K, (d) 473 K, (e) 523 K, and (f) 573 K in accordance with the X procedure. The NPs were synthesized using the mixed targets of $f_{Au} = 0.50$.

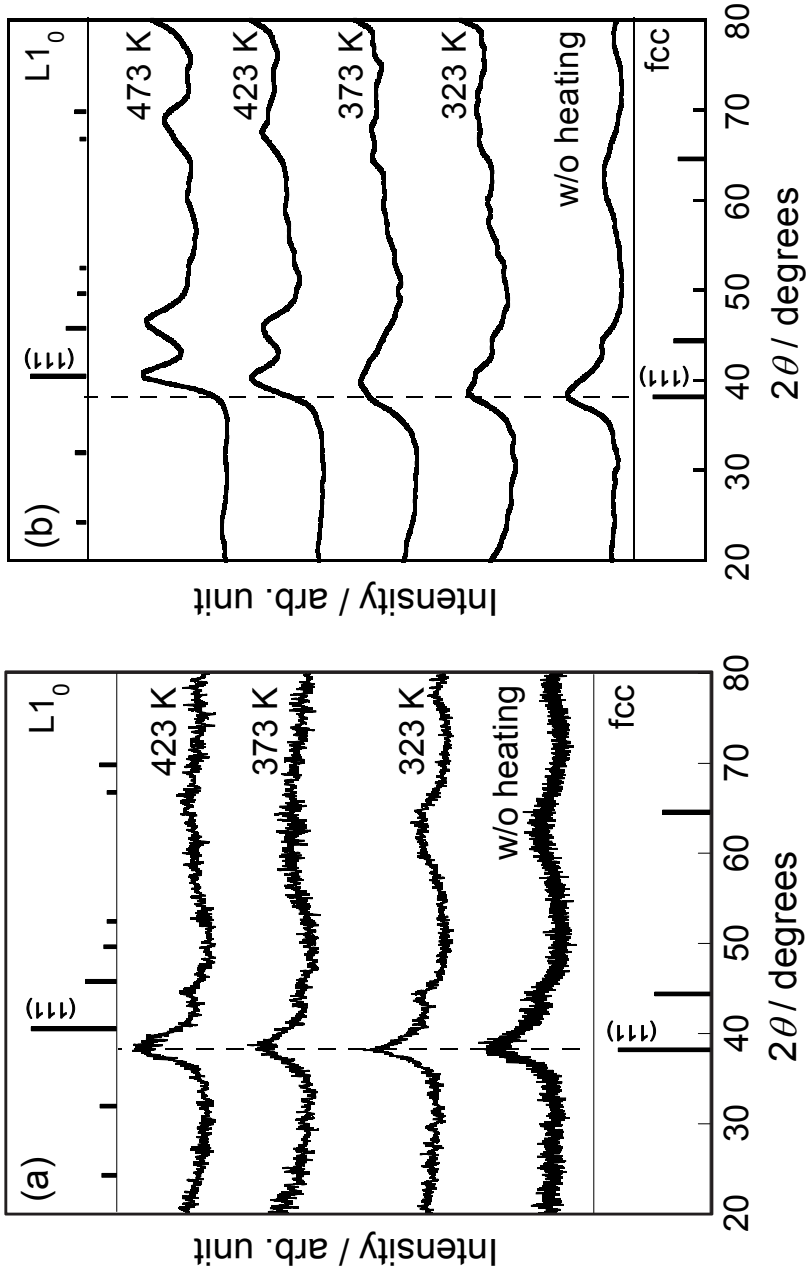

Fig. 7 XRD profiles of the NPs obtained (a) by application of heating during the sputter deposition and (b) by application of the continuous heating for 1 h after the sputter deposition through the Y procedure. Cases without heat treatment are also shown in these figures. The bar graphs in each figure at the bottom and the top are references describing the peak positions of the fcc structure and the $L1_0$ structure, respectively. A dashed line in each figure shows the (111) peak position in the fcc structure. The NPs were synthesized using the mixed targets of $f_{Au} = 0.50$.

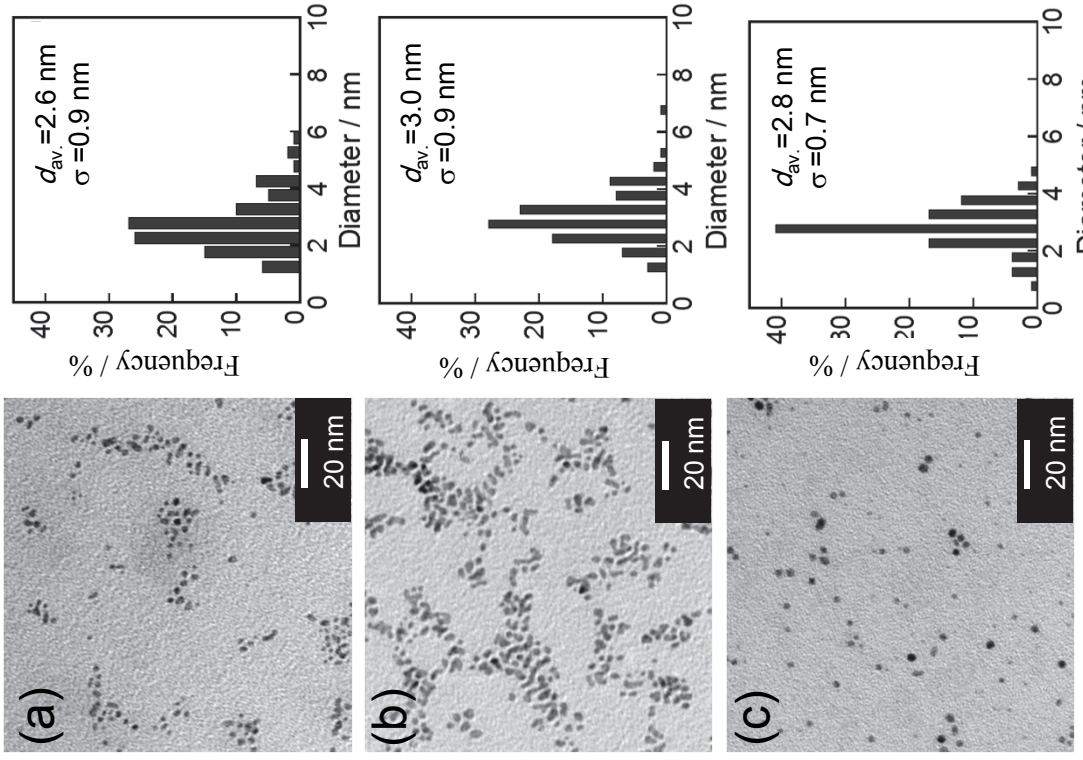

Fig. 8 TEM images and size distributions of NPs obtained through the first heating step in the Y procedure at (a) 323 K, (b) 373 K, and (c) 423 K. The heating as the first step was conducted during the sputter deposition onto the IL. The NPs were synthesized using the mixed targets of $f_{Au} = 0.50$.

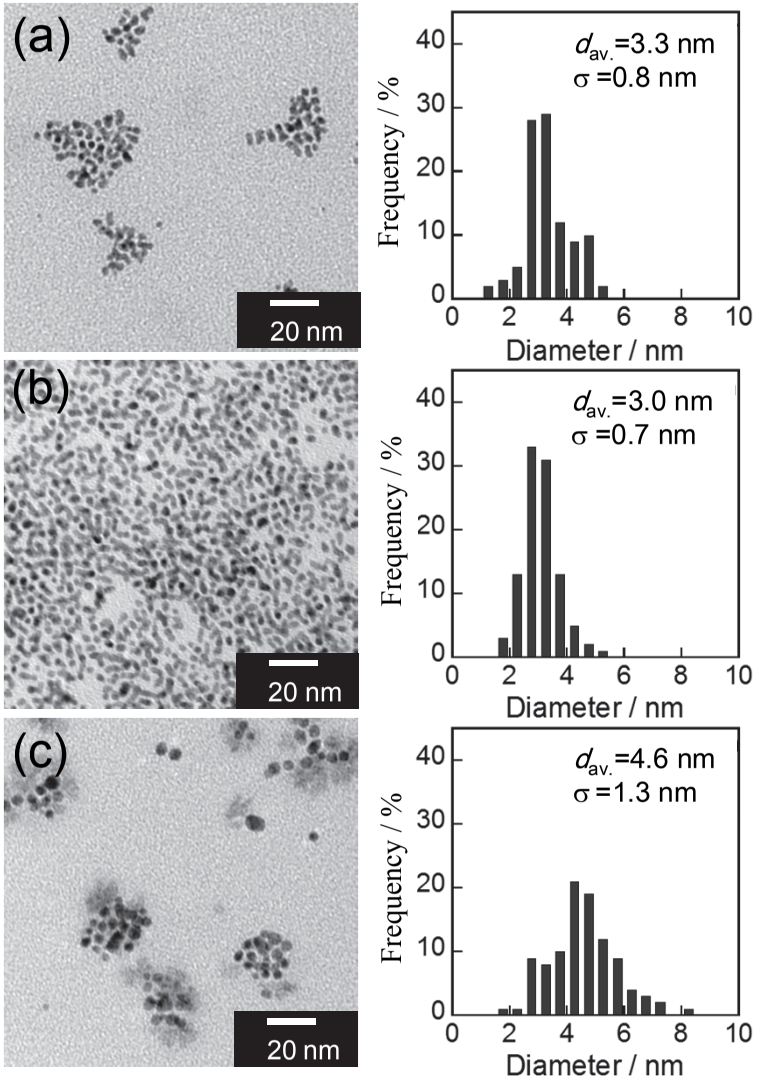

Fig. 9 TEM images and size distributions of NPs obtained through the whole process in the Y procedure at (a) 323 K, (b) 373 K, and (c) 423 K. The second step of subsequent heating was conducted for 1 h. The NPs were synthesized using the mixed targets of $f_{Au} = 0.50$.

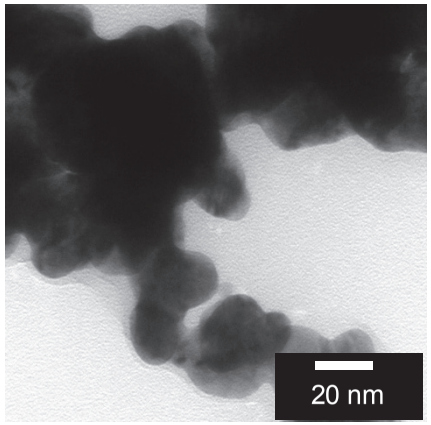

Fig. 10 TEM image of NPs obtained through the whole process in the Y procedure at 473 K. The NPs were synthesized using the mixed targets of $f_{Au} = 0.50$.

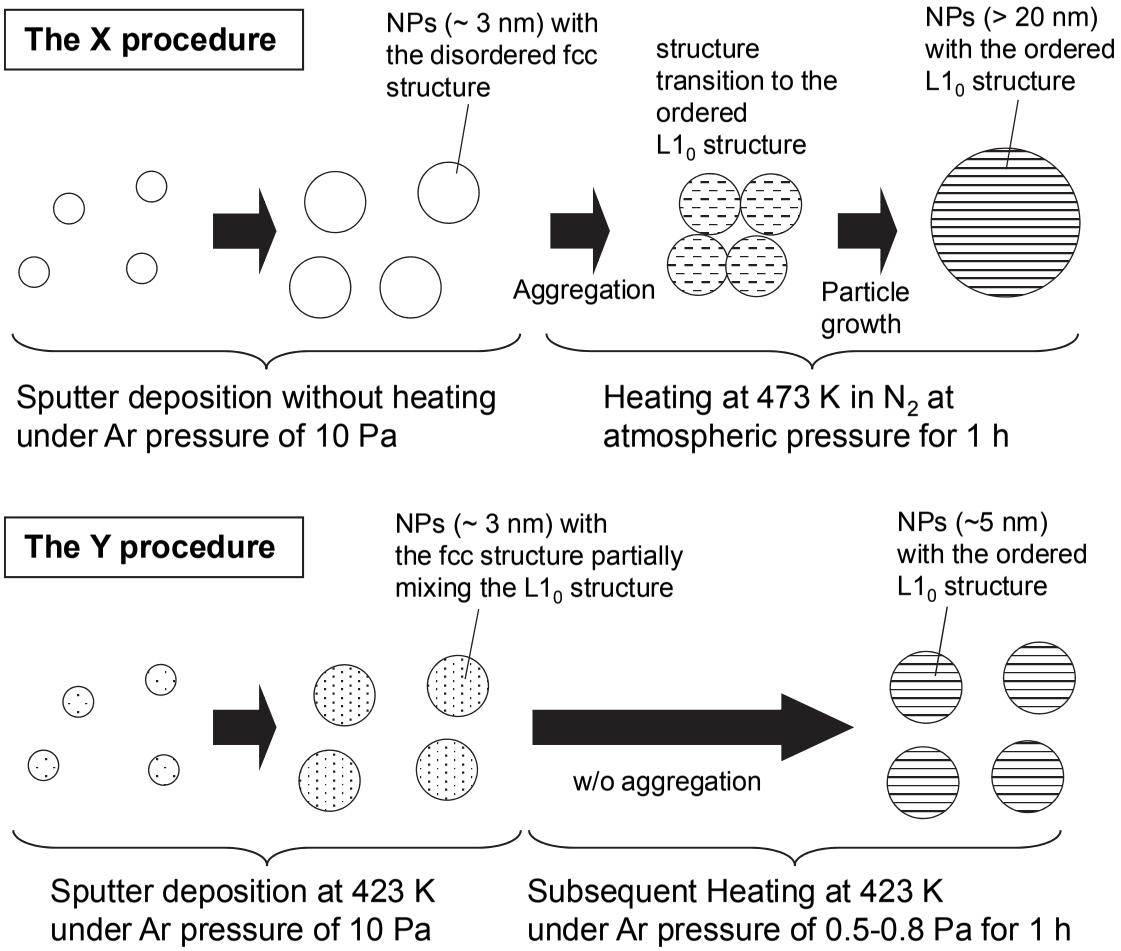

Fig. 11 Mechanism on the formation of the $L1_0$ structure in the AuCu alloy NPs in EMI-BF_4 by application of (a) the X procedure at 473 K and (b) the Y procedure at 423 K.

Graphical Abstract

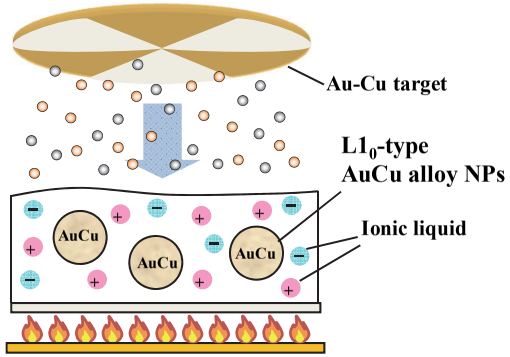

Synthesis of alloy AuCu Nanoparticles with the $L1_0$ Structure in an Ionic Liquid using Sputter Deposition